

Nanopantography: A New Method for Massively Parallel Nanopatterning over Large Areas

Lin Xu,[†] Sri C. Vemula,[‡] Manish Jain,[†] Sang Ki Nam,[†] Vincent M. Donnelly,^{*,†}
Demetre J. Economou,[†] and Paul Ruchhoeft[‡]

Department of Chemical Engineering and Department of Electrical and Computer Engineering, University of Houston, Texas 77204

Received October 5, 2005; Revised Manuscript Received October 27, 2005

ABSTRACT

We report a radically different approach to the versatile fabrication of nanometer-scale preselected patterns over large areas. Standard lithography, thin film deposition, and etching are used to fabricate arrays of ion-focusing microlenses (e.g., small round holes through a metal/insulator structure) on a substrate such as a silicon wafer. The substrate is then placed in a vacuum chamber, a broad-area collimated beam of ions is directed at the substrate, and electric potentials are applied to the lens arrays such that the ions focus at the bottoms of the holes (e.g., on the wafer surface). When the wafer is tilted off normal (with respect to the ion beam axis), the focal points in each hole are laterally displaced, allowing the focused beamlets to be rastered across the hole bottoms. In this “nanopantography” process, the desired pattern is replicated simultaneously in many closely spaced holes over an area limited only by the size of the broad-area ion beam. With the proper choice of ions and downstream gaseous ambient, the method can be used to deposit or etch materials. Data show that simultaneous impingement of an Ar⁺ beam and a Cl₂ effusive beam on an array of 950-nm-diam lenses can be used to etch 10-nm-diam features into a Si substrate, a reduction of 95x. Simulations indicate that the focused “beamlet” diameters scale directly with lens diameter, thus a minimum feature size of ~1 nm should be possible with 90-nm-diam lenses that are at the limit of current photolithography. We expect nanopantography to become a viable method for overcoming one of the main obstacles in practical nanoscale fabrication: rapid, large-scale fabrication of virtually any shape and material nanostructure. Unlike all other focused ion or electron beam writing techniques, this self-aligned method is virtually unaffected by vibrations, thermal expansion, and other alignment problems that usually plague standard nanofabrication methods. This is because the ion focusing optics are built on the wafer.

Miniaturization technology has been driven almost exclusively by the semiconductor industry. Without question, the smallest and most complicated devices ever engineered are the integrated circuits that are being manufactured today throughout the world. The widths of features on these circuits are as small as 90 nm, whereas the thicknesses of the layers are approaching one monolayer. The scaling laws of electron device physics and economics show little sign of letting up on the demand for continued reduction in feature size.¹ While this evolution continues, a realization has emerged that making things even smaller could have applications well beyond the conventional CMOS semiconductor integrated circuit.² Although ideas have so far outpaced developed applications, some promising results have been obtained. For example, extremely small transistors have been made from single carbon nanotubes.^{3–5} Significant advances have also been achieved in quantum wire⁶ and quantum dot devices⁷ including quantum-dot cellular automata.^{8,9} Large scale

production of these devices is impeded by the lack of a fast method of producing the very small features that are required.

The present method for making small features consists of lithographically defining polymeric resist materials and then transferring the developed pattern into the desired underlying deposited film or substrate by plasma etching. State-of-the-art immersion photolithography can produce features as small as 45 nm but is extremely complex and costly. Ion beam or electron beam proximity or projection lithography methods are capable of much finer resolution (tens of nm), but require expensive and fragile masks. The finest features are made by electron beam writing into resist. Although this method is very good for prototype devices, it is not practical for large-scale fabrication and production because the writing speed is much too slow to cover a several square centimeter chip size area, let alone a large wafer, in a reasonable time. Consequently, other methods have been sought to make devices with nanometer-sized features on a large scale.

One such approach is self-assembled monolayers (SAMs),^{10–13} which continues to be explored for fabrication of molecular-scale structures and devices. One motivation

* Corresponding author. E-mail: vmdonnelly@uh.edu.

[†] Department of Chemical Engineering.

[‡] Department of Electrical and Computer Engineering.

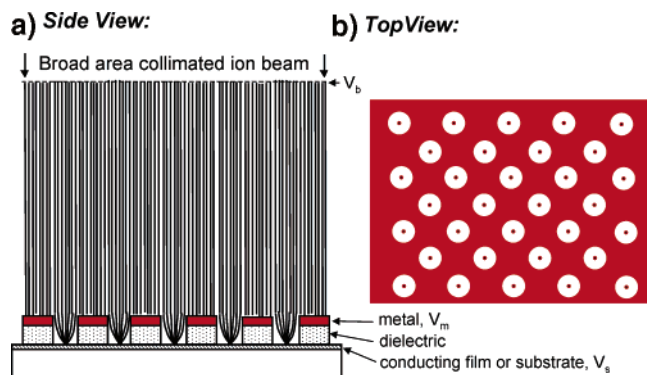


Figure 1. (a) Diagram depicting a collimated broad-area ion beam and substrate containing microlens arrays. The element at potential V_m could be a single conducting plate or multiple plates at various potentials separated by insulators. (b) Plan view showing a small region of an array of lens holes with a small feature deposited or etched in the center of each hole.

is construction of single molecule transistors.^{2,14,15} SAM films with larger dimensions (microns) are delineated by lithography or stamping.¹¹ Self-assembled structures can also be fabricated with block copolymers.^{16,17} This method can be used to make complex patterns with nanometer-sized features and varying length scales. A major breakthrough is needed, however, to make *any* desired pattern or three-dimensional shape in *any* desired material over a large area.

Here we report for the first time a new and radically different approach to nanometer-scale fabrication of preselected patterns over large areas. We use standard lithography, thin film deposition, and etching to fabricate an array of very small ion-focusing microlenses on a substrate (e.g., a silicon wafer). This array consists of small holes that can be arranged in any desired pattern. The substrate is then placed in a vacuum chamber and a positive voltage is applied to the top metal layer on the lens array. A broad-area collimated beam

of positive ions is extracted from a pulsed plasma and directed at the substrate, and the voltage on the microlenses is optimized by simulations and experiments such that the ions are focused at the bottoms of the holes (e.g., on the wafer surface), as depicted in Figure 1. At the focal points, inert ions such as Ar^+ can be made to cause rapid etching in the presence of reactive gases (e.g., Cl_2 for Si), while metal ions sputtered from a target electrode could be extracted and deposited at energies below the sputtering threshold.

As shown below, ions can be focused with 950-nm-diam lenses to a diameter of 10 nm, a size reduction of 95x. Because the electric fields within the lens scale with lens size (i.e., depth) and the transit time of ions traversing the field lines decreases as the lens size decreases, the problem is dimensionless if the lens aspect ratio and potentials are held constant. Consequently, it should be possible to produce a ~ 1 -nm-diam feature with 90-nm-diam lenses. Unlike all other focused ion or electron writing techniques, this method is virtually unaffected by vibrations, thermal expansion, and other alignment problems. This is because the ion focusing optics are mounted *on* the substrate.

Although etching or growing arrays of single, circular features in the centers of holes could have several applications (e.g., the nucleation of carbon nanotubes for field-emission displays or transistors), to realize the full potential of this method, consider what happens when the ion beam axis is moved off normal with respect to the wafer by tilting the beam or the wafer. Instead of focusing at the center of the hole bottoms, the focal points are displaced. Imagine the line normal to the wafer surface intersecting an imaginary horizontal plane at a distance of, for example, 1 m from the wafer (Figure 2). Because the wafer in this case is tilted in two orthogonal directions, the normal traces a pattern on the imaginary plane. This pattern is replicated by the ions that focus at the bottom of the holes, with a reduction of about

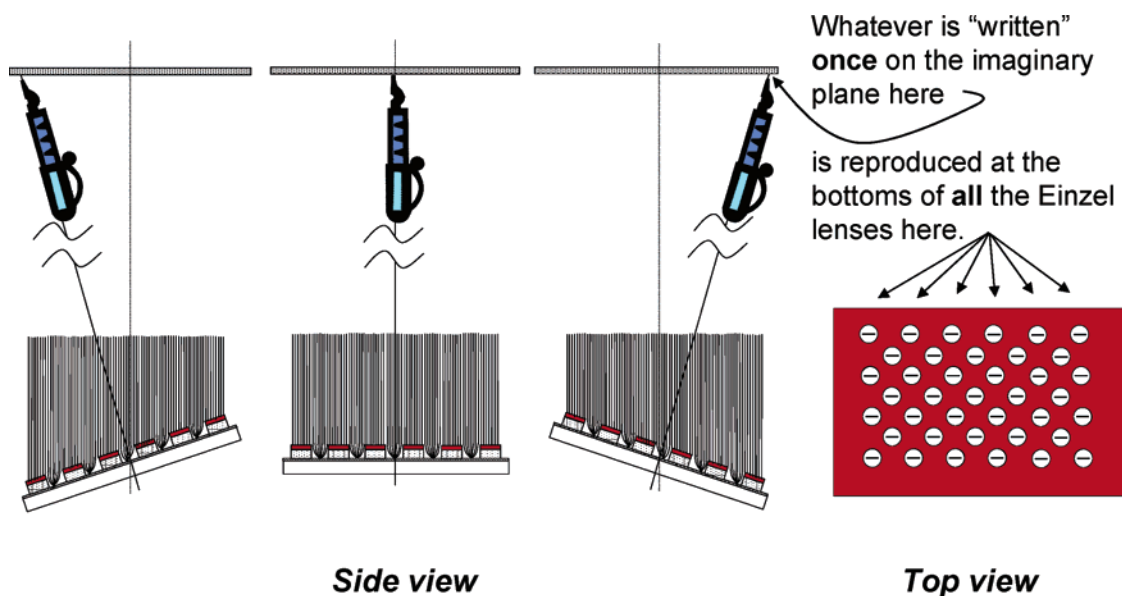


Figure 2. The nanopantography method. As the wafer is tilted about two orthogonal axes, the intersection of the wafer normal with an imaginary plane at far field traces a pattern that is written simultaneously at the bottoms of a large number of holes. In the above example (a) three positions are indicated as the wafer is tilted in one direction and a line is written, as depicted in b.

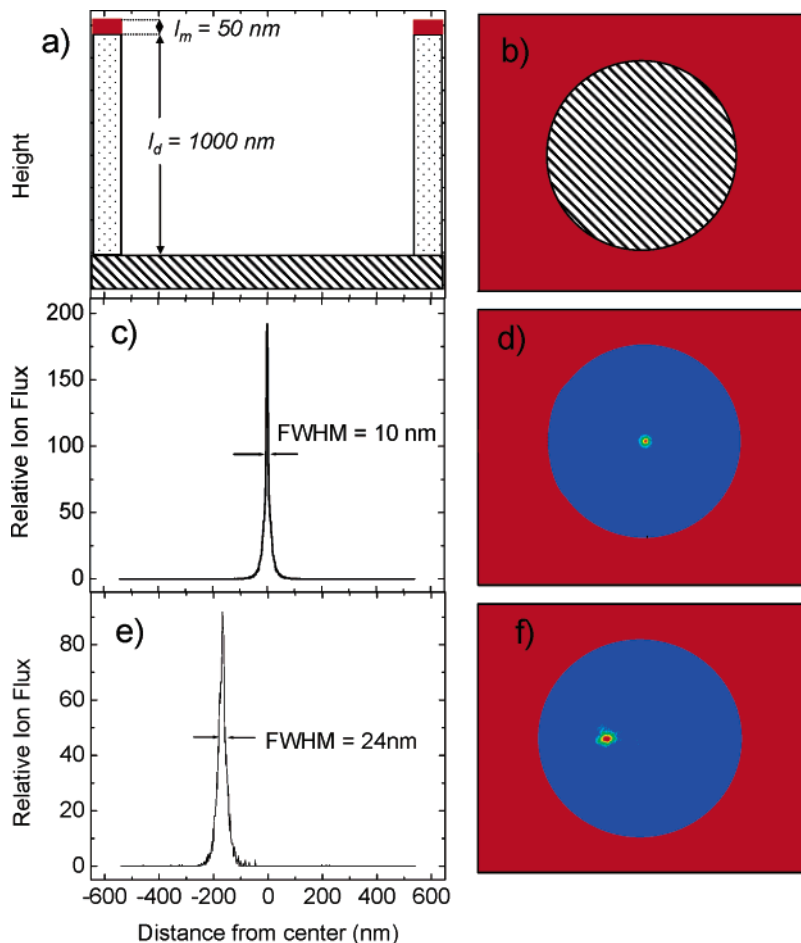


Figure 3. (a) Schematic of a single lens. (b) Simulations of relative Ar^+ flux as a function of distance across the bottom of a $d_m = 1080\text{-nm}$ -diam lens. Ion energy $E_i = 200\text{ eV}$, $V_m = 197.2\text{ V}$, $V_s = 100\text{ V}$, $l_m = 50\text{ nm}$, and $l_d = 1000\text{ nm}$. Ion beam axis is at normal incidence with respect to the substrate surface. (c) As in b but the ion beam axis was tilted by 20° , $V_m = 196.7\text{ V}$.

10^9 . This is the essence of nanopantography. The “dead” space between lenses is also available for larger scale circuitry, formed by conventional lithographic methods, to address and control discrete nanodevices or nanocircuits inside the holes.

Here we show that nanometer-sized features can be etched into Si with an Ar^+ ion beam, with Cl_2 background gas in the substrate chamber. We also envision this method being used to deposit metals and semiconductors or oxidize silicon (with an O_2^+ beam and surface charge neutralization). In principle, any preselected arbitrary pattern in a number of layers of materials can be achieved.

The nanopantography apparatus consists of an ion beam source region, an ion “drift” region, and a wafer processing region. A schematic of the apparatus is given in the Supporting Information. The ion source is a 13.56 MHz inductively coupled plasma reactor. The radio frequency (RF) inductive power is delivered through a 3 1/2-in.-diam 2-turn coil that is immersed in the plasma. The coil is fabricated from 1/4-in. o.d. nickel tubing and is water-cooled. The remaining aspects of the plasma reactor and ion beam source are the same as those for the capacitively coupled system described in a previous publication.¹⁸

Ions are extracted through a grid at the bottom of the plasma chamber. To obtain the best image resolution from

the broad-area ion beam, one must minimize the beam divergence angle ($\Delta\phi$) and kinetic energy spread (ΔE). This is achieved by pulsing the plasma on and off with a frequency of 5 kHz and a 50% duty cycle. During the power off fraction of the cycle, the plasma fields, RF plasma potential, and electron temperature quickly relax (within several μs), while the plasma density drops only moderately.^{19,20} After plasma relaxation, a positive, constant (DC) voltage is applied to a 4.4-in.-diam 0.3-in.-high ring electrode that surrounds the intense plasma region. The plasma potential shifts to this applied voltage. The ion beam energy, which is the difference between the plasma potential and the grounded grid potential, can thus be controlled precisely.¹⁸

The sample is exposed to the ion beam in a separate chamber that is 30 in. downstream from the extraction grid of the plasma source. A drift region is needed in between to reduce the gas number density, such that only a small fraction of the ions collide with the background gas. Two stages of differential pumping are used in the chambers that separate the plasma source from the substrate.

The ability to focus ions into the bottoms of cylindrical holes from parallel “beamlets” of a collimated broad-area ion beam is central to nanopantography. The beamlets are comprised of the ions that enter the tops of the holes. Each hole is a microlens, similar to electrostatic lenses in, for

example, focused ion beams or mass spectrometers, except for their small size. Unlike conventional ion projection lithography, there is no crossover point anywhere in the beam where a very high ion density creates a large enough space charge that distorts the beam.²¹ In our case, each lens contains on average only $\sim 10^{-5}$ ions. Therefore, the probability of two ions occupying a lens at the same time and repelling each other is extremely remote. In addition, because the lenses are on the wafer, there is no need for the critical alignment and vibration control that is required for the alternative approach of projection of multiple focused ion beams onto a scanned substrate.²²

The single element lens depicted in Figure 1 is the simplest form. Ions with a kinetic energy E_i pass through the grounded grid as they exit the source plasma and travel a total distance, l , where they encounter a metal electrode at a potential V_m , with a thickness l_m and having a through-hole of diameter d_m . Ions with proper trajectories to pass through this hole then pass through a hole with a diameter d_d in a dielectric material of thickness l_d . Here we make $d_d > d_m$ (see the Supporting Information) to eliminate the possibility of charging due to ions that may strike the sidewall.

The ions are deflected by the spatially varying potentials, and with the proper conditions come to a focus at the bottom of the hole (e.g., on the substrate surface). To obtain the best focus, we performed ion trajectory simulations to optimize the focal characteristics of the lens. As an example for comparison with one of the experiments below, we simulated a lens (Figure 3a and b) with $l_m = 50$ -nm-thick metal resting on top of $l_d = 1000$ -nm-thick insulator (silicon dioxide) on a silicon substrate. The hole diameter was $d_m = d_d = 950$ nm. The potential of the metal, V_m , was the control variable, while the substrate was at the reference potential (V_s , taken here to be 100 V). The volumetric charge density in the region around a single lens is negligibly small. Thus, the 2D Laplace equation was used to determine the potential and electric field profiles in the domain. A uniform flux of ions was launched at the entrance plane with the measured ion energy distribution. Using the electric field profile, the 3D trajectory of each ion was computed by integrating Newton's equation of motion with a leap-frog method. Integration continued until ions struck a surface.

Figure 3c and d shows the ion flux distribution along the radius at the bottom of the 1080-nm-diam hole when the ion beam axis is normal to the substrate surface. Very sharp focusing of the ion flux is predicted; the full width at half-maximum (fwhm) is 10 nm, that is, a reduction factor of 100x, compared to the hole diameter. In Figure 3e and f the ion beam axis is at an angle of $\phi = 20^\circ$ with respect to the surface normal (see Figure 2). The focal point is displaced by 167 nm. In this manner, any desired pattern may be "written" by tilting the wafer and rastering the beam over the bottom of the hole, as depicted in Figure 2. The feature width broadens somewhat with tilt angle (fwhm = 24 nm at $\phi = 20^\circ$) with this nonoptimized single-stage lens structure.

Samples were exposed to a 200 or 100 eV Ar^+ and a Cl_2 effusive beam with an estimated Cl_2/Ar^+ flux ratio of 200:1. Under these conditions, Si will etch at a rate of 1.3 Si

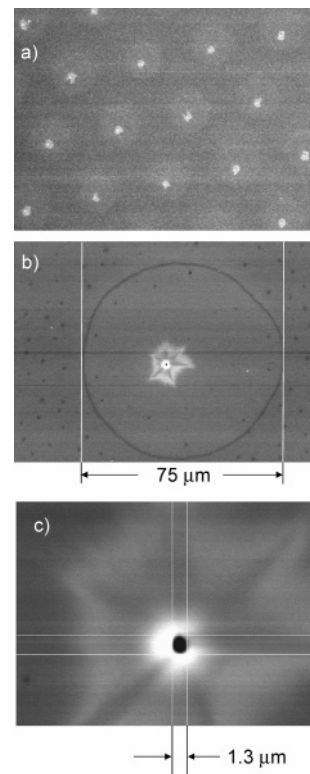


Figure 4. Scanning electron micrographs of patterns etched into Si with a stencil mask lens array. $d_m = 75$ - μm -diam lens. $E_i = 200$ eV, $V_m = 188.9$ V, $V_s = 0$ V, $l_m = 50$ μm , and $l_d = 100$ μm . The stencil mask and dielectric layer have been removed. The etched hole depth is 1 μm .

atoms per Ar^+ at $E = 200$ eV²³ and 0.7 Si atoms per Ar^+ at $E = 100$ eV.²⁴ The sputtering rate in the absence of Cl_2 is much slower (0.3 and 0.1 Si atoms per Ar^+ at $E = 200$ and 100 eV, respectively).²⁴ Spontaneous etching of Si by Cl_2 is very slow at room temperature; hence, etching occurs only at the focal points of the Ar^+ beamlets. Etched samples were examined by high-resolution top-down scanning electron microscopy (SEM) and atomic force microscopy.

First, a proof-of-principle experiment was carried out using a metal foil with a closely spaced pattern of 75- μm -diam holes. Figure 4a is an SEM of a small portion of the pattern formed after etching and removal of the foil and spacer. Faint outlines of the lenses are visible as well as features inside each lens. (The lens outline is from a subtle transformation of the Si surface, induced by fast neutral species, the Cl_2 gas, and/or ultraviolet light from the plasma.) Figure 4b more clearly shows the outline of a single lens and the feature etched by the focused ion beamlet. The sixfold "star pattern", although indicating some distortion (perhaps from radial asymmetry induced by the hexagonal array), is nonetheless very shallow relative to the deep depression at the center. Figure 4c shows this region greatly expanded. The etched hole diameter measured with the SEM is 1.3 μm , resulting in a reduction factor of ~ 60 x, compared to the 75- μm lens diameter. AFM scans indicate that the holes are 1 μm deep, with a diameter of ~ 2.8 μm near the top and a width (fwhm) of 1.2 μm .

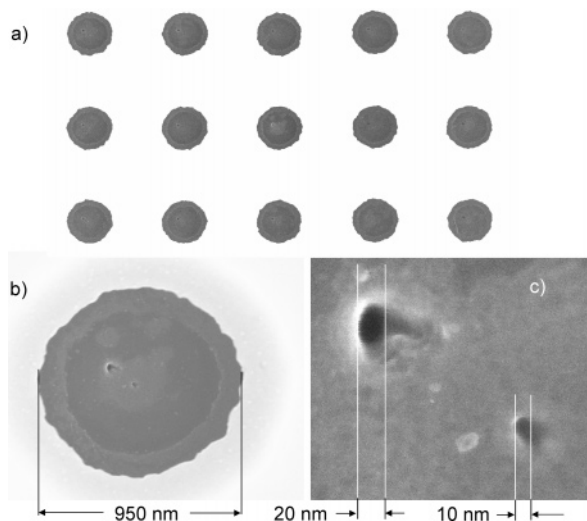


Figure 5. Scanning electron micrographs of patterns etched into Si with a Cr/SiO₂/Si lithographically defined lens array. $d_m = 950$ -nm-diam lens. $E_i = 200$ eV, $V_m = 196$ V (normal incidence ion beam) or 195 V (20° off normal ion beam), $V_s = 100$ V, $l_m = 50$ nm, and $l_d = 1000$ nm. The off-axis hole, shown magnified in b and c, was etched with an angle between the ion beam and wafer surface normal of $\sim 20^\circ$. The on-axis hole, visible near the center in b and in the lower right corner in c, was etched with a beam at near normal incidence. Cr and SiO₂ are in place.

Next, a lithographically defined Cr/SiO₂/Si lens array with 700–1100-nm-diam holes was exposed to the same conditions as above. A small portion of the array, a single lens, and two etched holes at the bottom of the lens are shown in Figure 5a–c. The larger (20-nm-diam) off-axis hole corresponds to an estimated angle between the ion beam and the wafer normal of $\sim 20^\circ$. The 10-nm-diam on-axis hole corresponds to a separate experiment with near normal incidence of the beam. (Transverse electric fields in the drift region in the present system deflect the beam off normal and make it difficult to determine the precise angle.) The minimum spot size was quite sensitive to changes (± 2 V) in V_m and to lens diameter. At the optimum voltage for a 950-nm-diam lens (196 V, with a Si substrate potential of 100 V), the beamlets focus at the center and etch holes with diameters as small as 10 nm, resulting in a size reduction factor of 95x. Given the high degree of “waviness” at the edge of the Cr openings (because of the imprecise wet etching of the Cr layer), this tight focus is quite remarkable. The SEM image is in excellent agreement with the size and shape of the on-axis as well as off-axis holes predicted from the simulations (Figure 3). We were not able to probe into these very small holes by an AFM. However, on the basis of preliminary transmission electron microscopy (TEM) measurements, we estimate that these features are at least 110 nm deep.

In conclusion, we have shown that a collimated broad-area ion beam can be simultaneously focused by an array of 950-nm-diam holes (fabricated on a wafer by standard lithography) to produce focused ion beamlets as small as 10 nm in diameter that can be rastered across the bottoms of the holes and thus create massively parallel nanostructures.

We have demonstrated this concept by etching holes into Si with Ar⁺ beamlets in the presence of Cl₂ gas. This nanopantography process presents a viable method for overcoming one of the main obstacles in practical nanoscale manufacturing: rapid, repetitive fabrication of nanostructures of virtually any desired pattern over large areas. The possibility to etch and deposit materials, the natural self-alignment of the process, and the immunity from vibrations affords the possibility to fabricate nanostructures with novel physics and chemistry on the nanoscale, such as quantum dots, carbon nanotube arrays, and nanostructured catalysts.

Sharp ion focusing is obtained even with the simplest possible design of lens. Although experiments so far have shown a size reduction factor of 60–95x, simulations predict reduction factors of more than 100x even for these single element lenses. Hence, it should be possible to produce ~ 1 -nm features using a 100-nm-diam lens. The use of multiple element lenses should result in even better focusing and higher reduction factors. The fact that the reduction factor is independent of lens size indicates that, regardless of the achievable resolution of current lithography, nanopantography can improve this resolution by a factor of up to 100.

Acknowledgment. This research was supported by the National Science Foundation (NSF–NIRT-0303790). We thank Alain Diebold and Hugo Celio for TEM measurements.

Supporting Information Available: Additional materials and methods. This material is available free of charge via the Internet at <http://pubs.acs.org>.

References

- (1) Jeong, M.; Doris, B.; Kedzierski, J.; Rim, K.; Yang, M. *Science* **2004**, *306*, 2057.
- (2) Flood, A. H.; Stoddart, J. F.; Steuerman, D. W.; Heath, J. R. *Science* **2004**, *306*, 2055.
- (3) Tans, S.; Verschuere, A.; Dekker, C. *Nature* **1999**, *393*, 49.
- (4) Martel, R.; Schmidt, T.; Shea, H. R.; Hertel, T.; Avouris, P. *Appl. Phys. Lett.* **1998**, *73*, 2447.
- (5) Keren, K.; Rotem, S.; Buchstab, E.; Sivan, U.; Braun, E. *Science* **2003**, *302*, 1380.
- (6) Hopkins, D. S.; Pekker, D.; Goldbart, P. M.; Bezryadin, A. *Science* **2005**, *308*, 1762.
- (7) Rastelli, A.; Stuffer, S.; Schliwa, A.; Songmuang, R.; Manzano, C.; Costantini, G.; Kern, K.; Zrenner, A.; Bimberg, D.; Schmidt, O. G. *Phys. Rev. Lett.* **2004**, *92*, 166104.
- (8) Wang, K. L.; Liu, J. L.; Jin, G. J. *Cryst. Growth* **2002**, *237*, 1892.
- (9) Kummamuru, R. K.; Timler, J.; Toth, G.; Lent, C. S.; Ramasubramaniam, R.; Orlov, A. O.; Bernstein, G. H.; Snider, G. L. *Appl. Phys. Lett.* **2002**, *81*, 1332.
- (10) Whitesides, G. M.; Laibinis, P. E. *Langmuir* **1990**, *6*, 87.
- (11) Wilbur, J. L.; Whitesides, G. M. In *Nanotechnology*; Timp, G., Ed.; Springer-Verlag: New York, 1999; pp 331–369.
- (12) Gai, Z.; Wu, B.; Pierce, J. P.; Farman, G. A.; Shu, D. J.; Wang, M.; Zhang, Z. Y.; Shen, J. *Phys. Rev. Lett.* **2002**, *89*, 235502.
- (13) Lu, W.; Salac, D. *Phys. Rev. Lett.* **2005**, *94*, 146103.
- (14) Reed, M. A. *Proc. IEEE* **1999**, *87*, 652.
- (15) Liang, W. J.; Shores, M. P.; Bochrath, M.; Long, J. R.; Park, H. *Nature* **2002**, *417*, 725.
- (16) Stoykovich, M. P.; Muller, M.; Kim, S. O.; Solak, H. H.; Edwards, E. W.; Pablo, J. J. d.; Nealey, P. F. *Science* **2005**, *308*, 1442.
- (17) Leiston-Belanger, J. M.; Russell, T. P.; Drockenmuller, E.; Hawker, C. J. *Macromolecules* **2005**, *38*, 7676.
- (18) Xu, L.; Economou, D. J.; Donnelly, V. M.; Ruchhoeft, P. *Appl. Phys. Lett.* **2005**, *87*, 041502.
- (19) Malyshev, M. V.; Donnelly, V. M.; Colonell, J. I.; Samukawa, S. J. *Appl. Phys.* **1999**, *86*, 4813.

- (20) Ramamurthi, B.; Economou, D. J. *J. Vac. Sci. Technol., A* **2002**, *20*, 467.
- (21) Melngailis, J.; Mondelli, A. A.; I. L. B., III; Mohondro, R. *J. Vac. Sci. Technol., B* **1998**, *16*, 927.
- (22) Berry, I. L.; Mondelli, A. A.; Nichols, J.; Melngailis, J. *J. Vac. Sci. Technol., B* **1997**, *15*, 2382.
- (23) Balooch, M.; Moalem, M.; Wang, W.-E.; Hamza, A. V. *J. Vac. Sci. Technol., A* **1996**, *14*, 229–233.
- (24) Chang, J. P.; Arnold, J. C.; Zau, G. C. H.; Shin, H.-S.; Sawin, H. H. *J. Vac. Sci. Technol., A* **1997**, *15*, 1853–1863.

NL051976I